

Modelling local winds over the Salento peninsula

Cristina Mangia¹, Paolo Martano¹, Mario Marcello Miglietta¹, Angela Morabito^{1,2}
& Annalisa Tanzarella^{1,2}

¹Consiglio Nazionale delle Ricerche-Istituto di Scienze dell'Atmosfera e del Clima sezione di Lecce ISAC-CNR, Strada provinciale Lecce-Monteroni km 1.200 73100 Lecce (Italy)

Email: mangia@isac.cnr.it

²University of Lecce, Department of Science of Materials, Strada provinciale Lecce-Monteroni km 1.200 73100 Lecce (Italy)

A three-day mesoscale numerical simulation has been performed over the narrow Salento peninsula (south-eastern Italy) during summer conditions characterised by weak synoptic forcing. These atmospheric conditions favour the development of complex sea-breeze systems and convergence zones on the peninsula. The aim of this work is to investigate the ability of an atmospheric mesoscale model to reproduce the surface fields of meteorological variables in the presence of local-scale forcing and breeze circulations, which are fundamental in applications such as air pollution modelling and nowcasting.

The modelled fields have been compared with available surface measurements and sodar data. Results indicate that the model can simulate the general mean wind field in a realistic way. The diurnal evolution of the wind is well reproduced and the maximum deviations mostly occur during the night, being associated with calm conditions.

Statistical analysis indicates that the typical mean bias is found to be about 1 m s^{-1} for hourly averaged wind speed, less than 20° for wind direction and about 1°C for temperature. The root mean square error (rmse) varies from 1 to 3 m s^{-1} for wind speed, from 50° to 70° for wind direction, and is about 2.4°C for temperature. All the values of the numerical indexes are within ranges which are characteristic of those found for other state-of-the-art models applied to similar cases studies.

Despite a good overall agreement between predictions and observations, some discrepancies were found in the individual profiles due both to the limited spatial representation of the local details and to the complex wind field which makes the space-time matching between the model and the observations quite critical.

The structures of the thermal mixed layer and the breeze convergence zone are similar to numerical studies relative to more idealised conditions.

1. Introduction

Surface winds in coastal environments represent a challenge for meteorology on a local scale. This is because of large horizontal and vertical variations of meteorological parameters caused by the differential diurnal heating cycle at the sea/land boundary (Melas et al. 2000). In particular, on flat straight peninsulas, the development and overlapping of different thermal circulations leads to small-scale temporal and spatial variations of the wind field and of the boundary layer structure. Several studies on the effects of breeze interaction on coastal sites have been published (e.g. Bobyey et al. 1991; Nicholls et al. 1991) and an interesting and exhaustive 2D numerical study on the

effect of land width on the merging and convergence of breezes was performed by Xian & Pielke (1991).

Local variations induced by these circulations can have important practical consequences on local weather conditions and boundary layer structure, significantly modifying the dispersion of air pollutants (Fisher 2002).

Mesoscale prognostic and dispersion models have been developed significantly in the last few years; at the same time, increasingly affordable and accessible high-performance computing has become widely available. Thus the computational power offered by common computers is enough to enable meteorological models to run sufficiently fast in cascade with dispersion models

and to provide real-time predictions of the transport and dispersion of air pollutants (Lyons et al. 1995; Pielke & Uliasz 1998; Brandt et al. 2001).

However, as shown in many papers, the meteorological variables used in air quality models can contain significant errors. They can thus contribute to uncertainties in air pollution predictions, which are even larger than those associated with chemical rate constants (Sistla et al. 1996; Lyons et al. 1995; Seaman 2000). For this reason, the evaluation of mesoscale meteorological models is the first important step towards achieving more accurate dispersion simulations.

The aim of this work is to investigate the performance of a mesoscale meteorological model in reproducing the sea-breeze systems which form over the Salento peninsula. This is a narrow, flat area in the south-eastern part of Italy with two big industrial complexes on opposite coastlines.

The study focuses on the average characteristics of the wind field and boundary layer structure during typical summer conditions characterised by weak synoptic forcing and clear skies. Model results are compared with measurements from surface meteorological stations and sodar profiles.

2. Geographical and meteorological scenario

2.1. Description of the area

The Salento peninsula is located in south-eastern Italy, effectively dividing the southern Adriatic Sea from the northern Ionian Sea at the Otranto Strait (Figure 1). The peninsula is long and narrow: about 100 km long in a NW–SE direction, with an average width of 30–40 km.

The topography is generally flat with small hills: the maximum altitude (less than 200 m) occurs along the central axis of the southern part. Therefore, the effect of orography on the flow is weak and the region is influenced, along its entire coastal perimeter (about 200 km), mainly by complex sea–land breeze systems, caused by the diurnal heating cycle.

The presence of the Balkans, less than 200 km away, on the other side of the Otranto Strait, often produces a channelling effect on the wind, causing it to strengthen over the whole region. This occurs mainly when the wind comes from the north, under high-pressure conditions. Nevertheless, previous analyses of climatological time series showed that local forcing due to the thermal contrast between the land and the sea is always important in determining the wind distribution in the area (Martano 1996).

An important meteorological phenomenon, frequently observed on the Salento peninsula, is the convergence of sea breezes in the middle of the peninsula. Theoretical analyses of sea-breeze systems by Rotunno (1983) and Dalu & Pielke (1989) showed that the aspect ratio R of the phenomenon (i.e. the ratio between the horizontal and vertical length scale of the breeze front) is of the order of the Rossby radius N/f , where N is the Brunt-Väisälä frequency and f is the Coriolis parameter, sometimes substituted by the period of the diurnal heating (Steyn 1998), at a latitude of 41°N , and with a typical atmospheric lapse rate of $5^\circ\text{C}/\text{km}$, $R \approx 130$.

This means that, for a typical sea breeze height of several hundreds of metres, the inland breeze penetration can be tens of kilometres deep. Considering the small horizontal dimensions of the land mass of the Salento peninsula, breeze merging is to be expected over the area

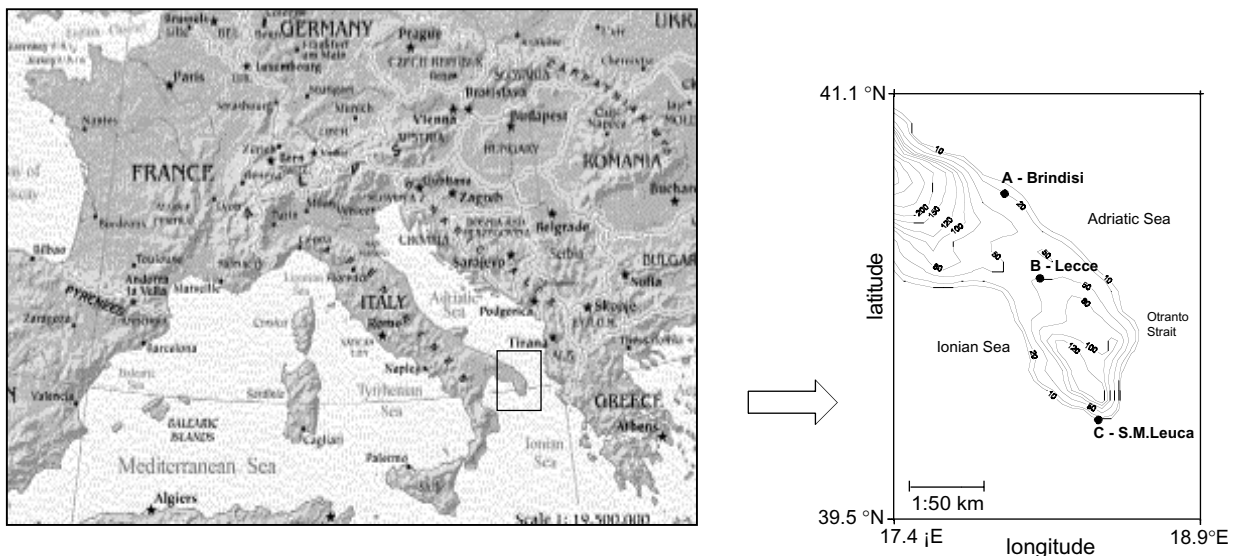


Figure 1. The Salento peninsula. Elevation contours (in m) are derived from topography used in the meteorological model. A, B and C represent the locations of measuring sites.

Table 1. Location of the meteorological stations. *Z* is the height relative to mean sea level. *Ws*, *wd*, *T*, *rh* indicate, respectively, wind speed, wind direction, temperature, relative humidity.

STATIONS	LAT.	LONG.	Z (m)	Measured quantities	Measurement heights (m)
A: Brindisi	40°39'	17°57'	3	ws, wd, T, rh	10
B1: Lecce	40°20'	18°6'	105	ws, wd, T, rh	10
B2: Lecce - sodar	40°20'	18°6'	105	ws, wd	40–610
C: S.M. Leuca	39°49'	18°21'	112	ws, wd, T, rh	10

and is often observed with a typical cloud stream along the peninsular axis.

In order to obtain a detailed description of the space variability of meteorological fields in the region, three meteorological stations situated in the area have been considered in this study. The position of each station is indicated in Figure 1. Stations A and C are, respectively, the Air Force meteorological synoptic stations of Brindisi and S. Maria di Leuca. They are equipped with standard instruments and the synoptic observations are stored routinely at intervals of three hours. In addition, rawinsondes are launched every 6 hours at Brindisi station, giving vertical profiles of meteorological fields. Station B belongs to the University of Lecce, and is located 5 km WSW from Lecce. Station B also has, in addition to traditional instrumentation, a sodar that produces boundary layer wind profiles from 40 m above the ground up to about 500 m with a resolution of 30 m.

Table 1 summarises the station locations and their characteristics. The distribution of the stations allows an evaluation of the spatial distribution of meteorological fields at three critical points, affected by different prevailing local wind breeze systems. This is evident by considering the wind climatology based on statistics compiled over 30 years, relative to the three stations for the month of June at 12UTC (Figure 2). At Station A, located on the Adriatic coast, a prevailing NNW component is observed (25%); moreover, all the components from NW to NE cover more than 50% of the total events. At Station B, located in the middle of the peninsula, two different breeze systems can be

distinguished, with a prevalence of Adriatic breezes (in more than 40% of cases the wind comes from N–NE), but with a significant presence of Ionian breezes (28% of cases are from 180° to 240°). Station C, located in the southern part and surrounded by sea, is characterised by complex wind circulations: a S–SW component prevails (almost 60% of the cases from SSE to WSW), with only 20% of winds being N–NW.

2.2. Synoptic conditions

The case study considered here examines the meteorological situation at 2–4 June 1998. The period is characterised by almost clear skies and weak synoptic forcing, which are favourable conditions for the formation of sea–land breeze systems. Figure 3 shows the NCEP/NCAR (National Centers for Environmental Predictions/National Center for Atmospheric Research) reanalysis maps, relative to the 500 hPa geopotential (Figures 3a and 3c) and to the sea level pressure (Figures 3b and 3d), respectively, for 2 and 4 June, 1200 UTC. On the first of these days, a wide ridge is present over the central Mediterranean Sea (Figure 3a), with a surface high pressure of 1018 hPa in Tunisia, Libya and Sicily (Figure 3b). Salento is on the eastern side of the ridge and is affected by a small surface pressure gradient, so that a weak north–western flow is present in the middle and upper troposphere, and a weak northern air flux at surface level. During the following days, the ridge moves toward the north–east (Figure 3c), affecting the central Mediterranean regions, and the geopotential gradient decreases. The presence of low pressure over the western Mediterranean Sea induces

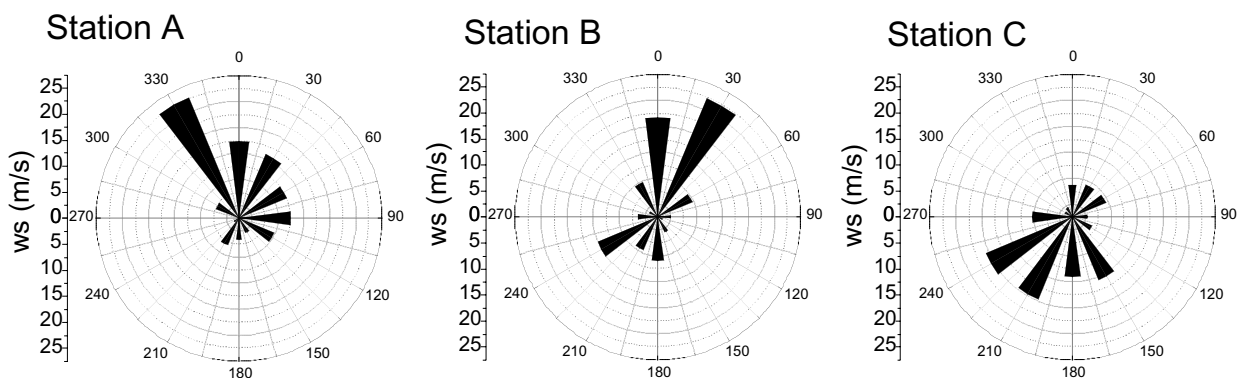


Figure 2. Wind roses for the month of June at 12 UTC, based on 30-year statistics, relative to the three meteorological stations.

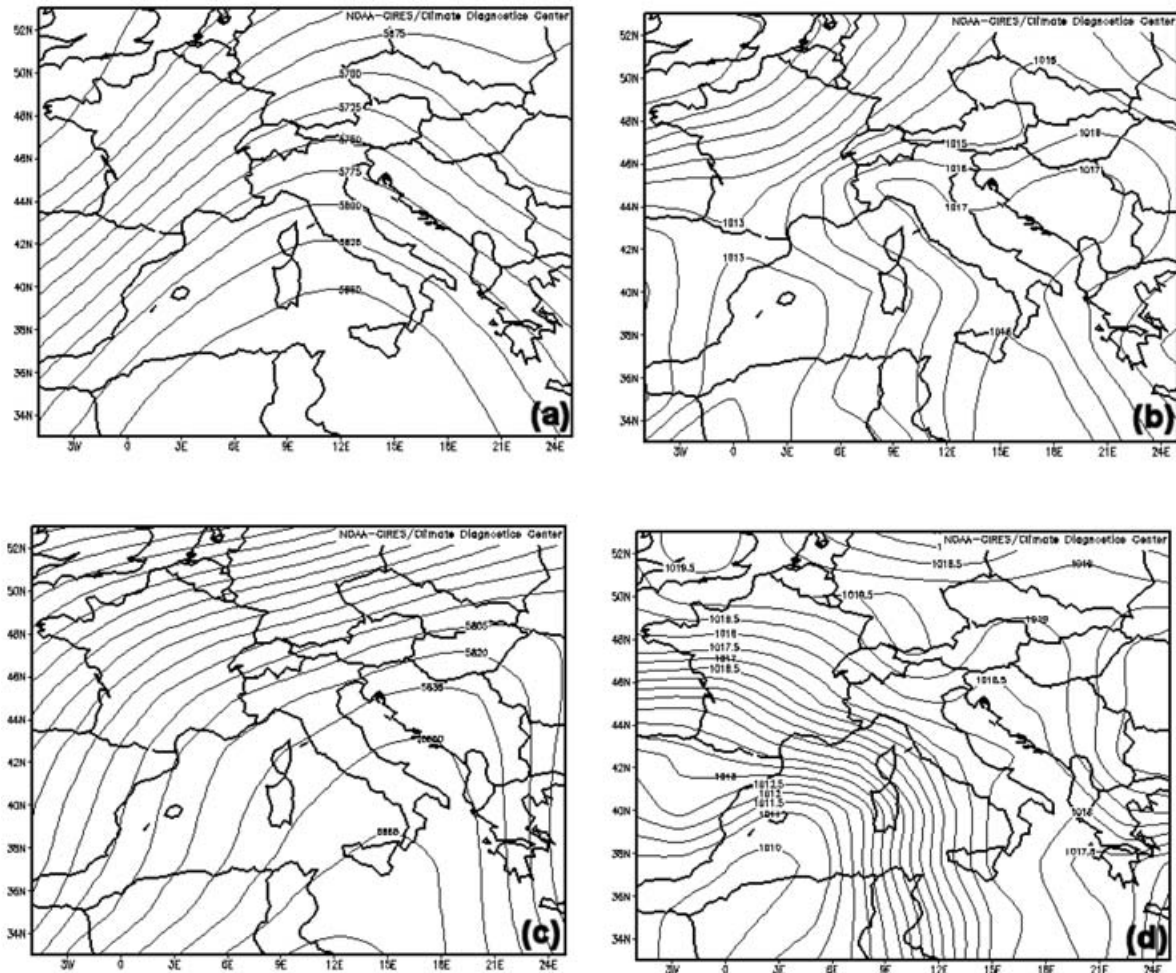


Figure 3. NOAA 500 hPa analysis for (a) 2 June 1998, 1200 UTC, and (c) 4 June 1998, 1200 UTC; NOAA mean sea level pressure analysis for (b) 2 June 1998, 1200 UTC, and (d) 4 June 1998, 1200 UTC.

a southern flow over south-west Italy (Figure 3d). However, a levelled pressure field still remains over south-eastern Italy: as will be shown later, this alteration in the synoptic flow implies a modification in the observed breeze patterns.

3. Model characteristics and setup

The simulations have been performed with the RAMS code version 3b (Pielke et al. 1992; Walko et al. 1995) in its non-hydrostatic version.

To improve spatial resolution, a two-way nested grid configuration is employed with three horizontal grids, each grid covering a different domain size (Figure 4). The coarsest grid has a mesh size of 36 km using 26×26 horizontal grid points. Grid b has a 12 km mesh size using 32×32 grid points. Grid c, the highest resolution grid, has a mesh size of 4 km with 32×44 grid points. In the vertical, the atmosphere is divided into 25 levels with different thicknesses, from 100 m starting near the surface, and then gradually stretching, at a fixed ratio of 1.2 up to the 13th level, to a maximum of 1000 m at the

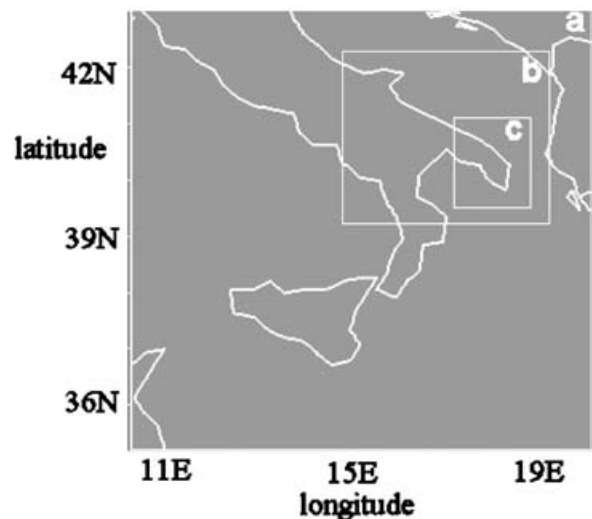


Figure 4. Domain of the three nested grids used for the simulation.

top (Table 2). Owing to the staggered grid system used in RAMS, the first vertical mesh point for the wind speed components is at a height of about 48 m. Horizontal

Table 2. Specification of the three grids used in RAMS. L_x , L_y and L_z are domain sizes in the x , y and z directions respectively; N_x , N_y and N_z are the number of mesh points in the x , y , and z directions, respectively; Δx and Δy are the mesh spacing in the x and y directions, respectively.

Grid	L_x (km)	L_y (km)	L_z (km)	N_x	N_y	N_z	$\Delta x, \Delta y$ (km)
1	936	936	15	26	26	25	36
2	384	384	15	32	32	25	12
3	128	176	15	32	44	25	4

domains and grids sizes have been designed so as to take into account both computational time limitations and the ability of the model to resolve essential mesoscale features.

For initial and boundary conditions, the Isentropic Analysis System (ISAN) package (the module of RAMS for the generation of data analyses) is used. At initial time, analysed fields are based on (i) the ECMWF gridded datasets, (ii) the rawinsonde upper air observations in station A, and (iii) the synoptic surface observations obtained from six different meteorological stations belonging to the Italian Air Force Meteorological Service (including stations A and C), distributed throughout the Apulia region. Every

6 hours, the lateral and the top boundary conditions in the coarsest grid are updated, using only the ECMWF gridded datasets. In the coarsest grid domain, a nudging towards the data is applied in the three grid points closest to the lateral boundaries and in the upper five grid levels. The impulsive initial introduction of the meteorological fields and of the topography creates an initial disturbance that is progressively damped as the meteorological fields adjust towards a state of quasi-equilibrium: to avoid any initial disturbance, we started the simulation one day before, i.e. 1 June.

In order to test the influence of sea surface temperature (SST) on the results, two different SST datasets have been used. The first is the RAMS SST dataset for June. The data, generated from monthly averages of 30 years (from about 1950 to 1980), originally came from the US Navy and is available with a resolution of $1^\circ \times 1^\circ$. The other dataset was obtained from daily NOAA satellite images, with a resolution of about 9 km, provided by the Physical Oceanography Distributed Active Archive Center (PODAAC).

Figure 5 compares the SST data from the two different datasets. Climatological data do not show differences in the temperature distribution between the two seas (Figure 5a), temperature varies from 21.2°C to 21.4°C . Satellite-derived SST data present more complex structures (Figure 5b): the Ionian sea temperature is

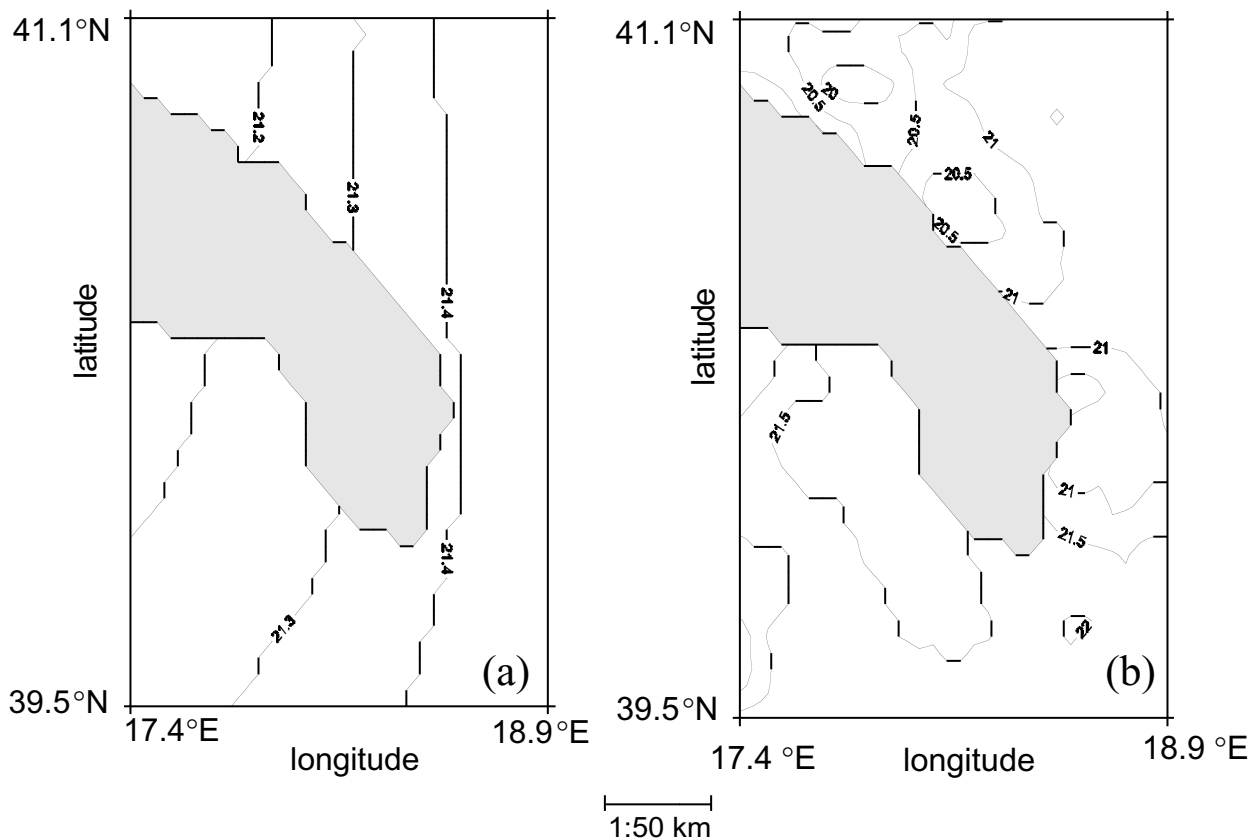


Figure 5. SST analysis for the two RAMS simulations in June 1998. (a) RAMS climatological data set; (b) data obtained from NOAA satellite images. Temperature data are given in $^\circ\text{C}$.

about 21.5°C – higher and more uniformly distributed with respect to the climatological data – whereas the Adriatic sea temperature is less uniform and varies from 20°C to 22°C with a difference of about $0.5\text{--}1^{\circ}\text{C}$ with respect to climatological data.

4. Results and discussion

4.1. Qualitative analysis

Figures 6, 7 and 8 show the modelled surface wind fields at two selected times that are representative of daytime

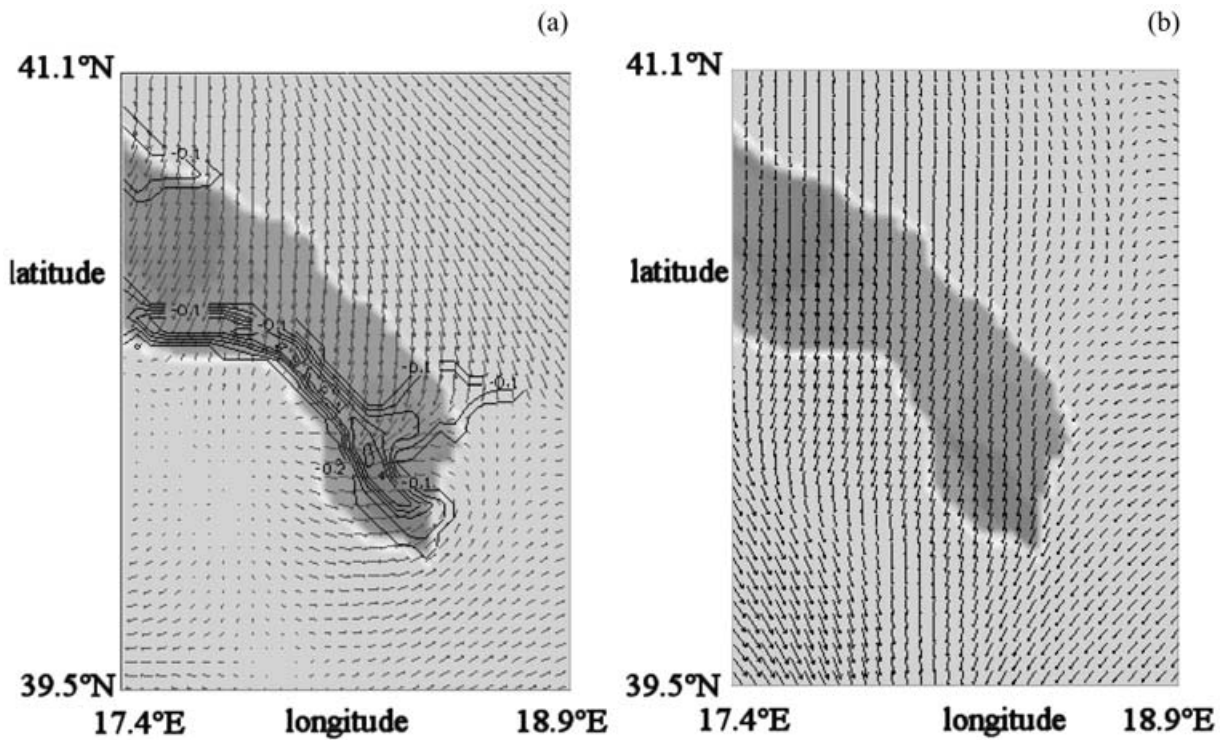


Figure 6. (a) Horizontal wind vectors (arrows) and isolines of vertical wind component at 250 m height at 14 UTC, 2 June; (b) horizontal wind velocity at 250 m height at 03 UTC, 3 June. Isoline interval is 0.1 m s^{-1} .

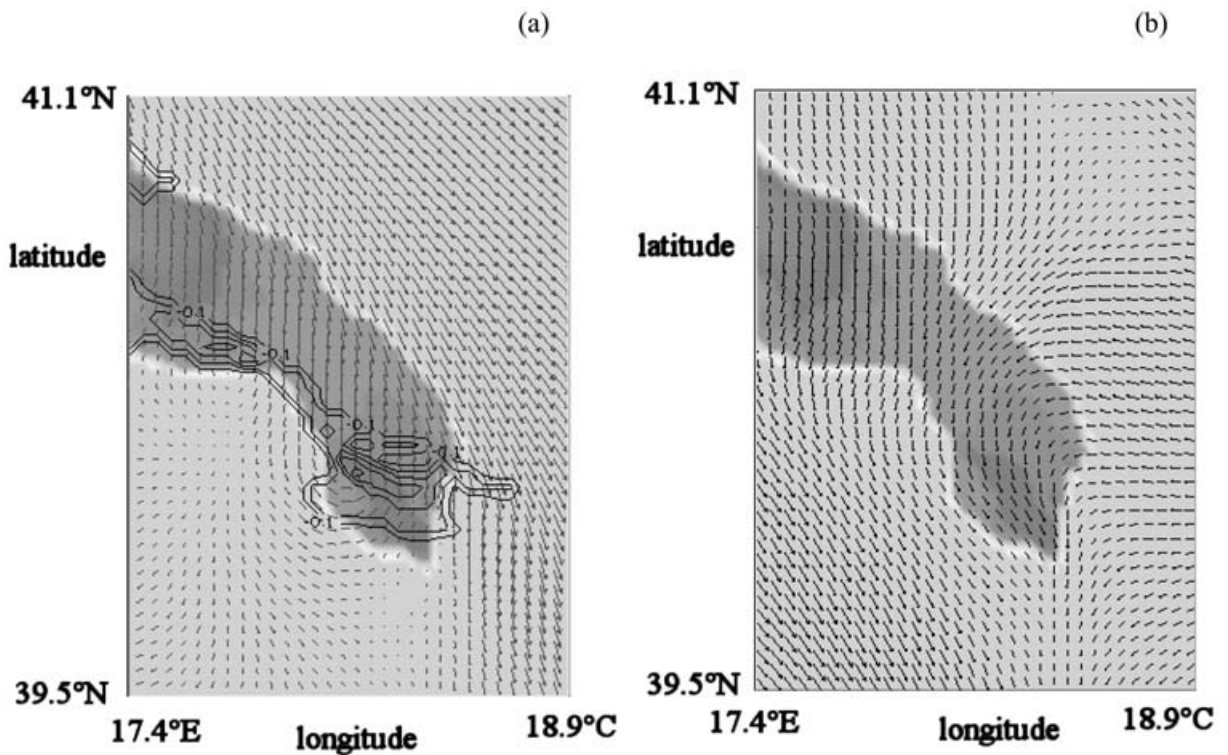


Figure 7. (a) Horizontal wind vectors (arrows) and isolines of vertical wind component at 250 m height at 14 UTC, 3 June; (b) horizontal wind velocity at 250 m height at 03 UTC, 4 June. Isoline interval is 0.1 m s^{-1} .

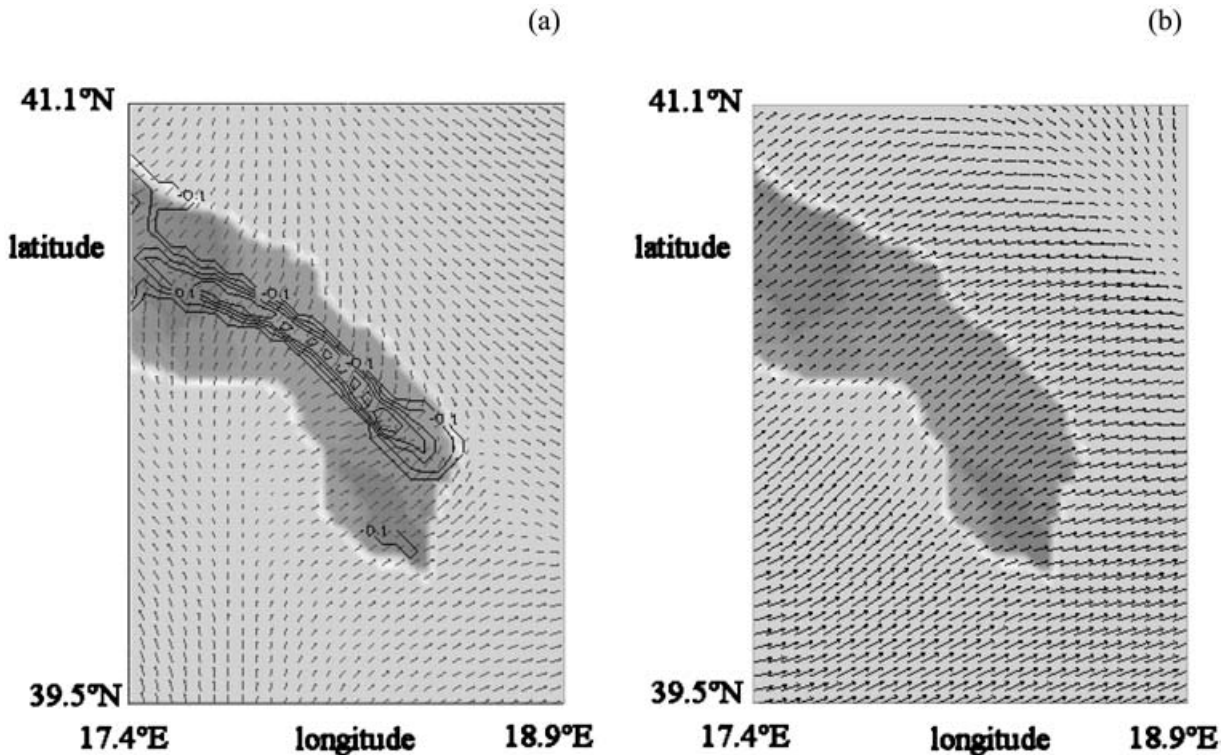


Figure 8. (a) Horizontal wind vectors (arrows) and isolines of vertical wind component at 250 m height at 14 UTC, 4 June; (b) horizontal wind velocity at 250 m height at 21 UTC, 4 June. Isoline interval is 0.1 m s^{-1} .

(14 UTC) and night-time conditions (03 UTC), 3 and 4 June; and 21 UTC, 4 June), respectively.

On 2 June, the weak synoptic north-western component, which affects the whole peninsula during the morning, rotates to WSW at Station C at 9 UTC, revealing the development of sea-breeze systems. At 14 UTC (Figure 6a), a very complex wind structure can be distinguished over the peninsula: a NW wind is observed along the Adriatic coast, which rotates to N-NE inland, next to the region of convergence, while a W-SW component is present along the Ionian coast. The convergence zone of the breezes shows the formation of a convective stream, as is clear from the isolines of vertical velocities. At 18 UTC, the simulation indicates that the sea-breeze circulation has ceased: convergence areas can no longer be detected, and during the night the wind remains weak and uniform over most of the peninsula (Figure 6b).

On 3 June, the presence of two distinct breeze systems can again be observed. The flow patterns at 14 UTC are shown in Figure 7a. In this case, the region of convergence is confined to the extreme southern part, since the SW breeze appears only in a narrow region close to the southern Ionian coast. Once again, the night-time wind presents a prevailing northern component over the entire peninsula (Figure 7b).

On 4 June, the synoptic situation changes, since a prevailing SW wind component is observed over

southern Italy, so that the northern forcing over Salento gradually disappears.

A prevailing south-western synoptic component can be observed at the end of the simulation (Figure 8b) over the entire third grid domain. As a consequence of the weakening of the northern forcing during the day, the convergence area is, in this case, much closer to the Adriatic coast than before, almost centred above the peninsula axis, as shown in Figure 8a. This stream persists in this location for several hours (approximately 12–16 UTC). Its displacement with respect to the case of 2 June, according to the synoptic wind conditions, has already been commented on in other publications (e.g. Xian & Pielke 1991) and is sometimes observed in the region through the formation of cloud streams.

Figures 9a and 9b show three E-W vertical sections for potential temperature and vertical velocity relative to 14 UTC, 4 June. From these it emerges that the mixed layer structure of the potential temperature is similar to the idealised case studied by Xian & Pielke (1991) in their 2D simulation of breeze merging over a land stream, for both variables. For vertical velocity the quantitative values lie in the interval found between the 24 km and 50 km landwidth simulations in the aforementioned paper. The convergence zone appears somewhat higher in the present simulation, probably because of the effect of the third dimension (finite along-axis extension of the peninsula, causing additional breeze forcing, and non-zero along-axis wind

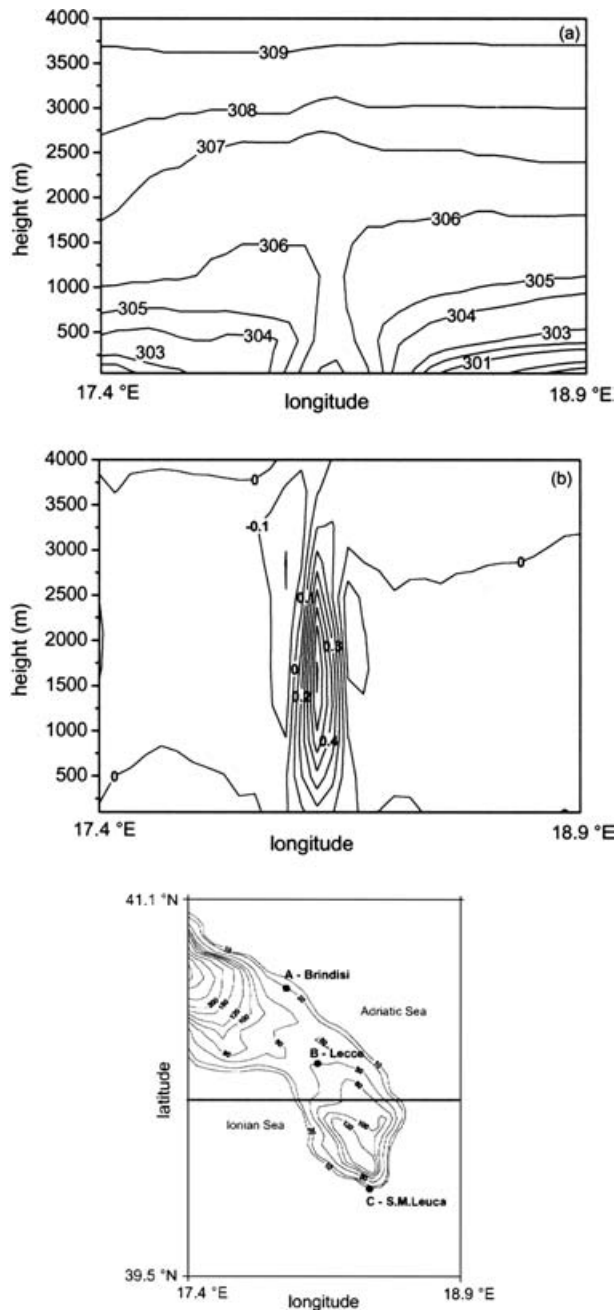


Figure 9. Isolines of (a) the potential temperature ($^{\circ}\text{K}$), and (b) the vertical velocity (m s^{-1}) for the W-E vertical section $40^{\circ} 20' \text{N}$ over the third grid at 14 UTC, 4 June. Corresponding topography is plotted at the bottom.

component, with enhanced fetch). From this figure it is also clear that the mixing height is affected by the breeze convergence, increasing up to about 2000 m in the convergence zone while, outside that region, a shallower boundary layer is usually found (Anthes 1978; Martano 2002).

4.2. Comparison with observations

4.2.1. Local time series

In order to compare observed data with model results, it must be recognised that (1) the measurements are

taken at discrete locations, while the calculated values are representative for a horizontal grid cell of $4000 \times 4000 \text{ m}$, and (2) the lowest sigma level is located 48 m above ground level. Thus the meteorological values produced by RAMS over that level need to be adjusted at the height of the observations, which is 10 m, by using standard boundary layer profile formulas (Stull 1988).

In addition, comparisons between observations and model predictions are complicated by the fact that observations are point measurements while model predictions are Reynold's average mean state variable.

Figure 10 shows the time variation of the modelled and observed wind speed and direction at the three stations for the period 2–4 June 1998. The thick line indicates RAMS simulations with the climatological SST; the thin line indicates model results with the SST satellite data. Differences in the simulated wind fields with the two SST datasets are small. For all the stations, a diurnal wind cycle with more or less pronounced variability is evident. The results for Station C are the worst. This could be due to the geographical position of Station C, which is situated at a height of 100 m relative to mean sea level and close to the sea, and due to the poor topographic resolution of the model which identifies Station C as a marine station. Figure 11 shows the modelled and sodar wind speed and direction at three different measurement heights. The wind direction follows the diurnal evolution moderately well, perhaps better as the measurement height increases. Such an improvement can be attributed to the decrease in local surface effects on the measured data. The wind speed seems to be underestimated by the model in particular during the day on 3 and 4 June.

Figure 12 shows the temperature and humidity evolution for the simulated period. The model is able to reproduce the spatial and temporal evolution of temperature for stations A and B quite well, but it is not able to reproduce the temperature excursion for Station C correctly. Again, the position of Station C could be responsible for the discrepancy, due to its actual height, its exposure and its sensitivity to very local advection effects from different directions. Analysis of Figures 10 and 12 indicates that the relative humidity data are the most sensitive to the SST dataset: predictions improve by using SST satellite data, as a consequence of the increased resolution.

A statistical analysis of model results, or more precisely, of the differences between measurements and predictions, has been performed. The statistical root mean square error and the bias have been considered as performance indexes (Hanna & Yang 2002). These measures are given both as relative values (normalised mean square and fractional bias), with their original absolute units and values normalised by the observed and predicted averages, for each meteorological variable that has been considered (wind, temperature, relative

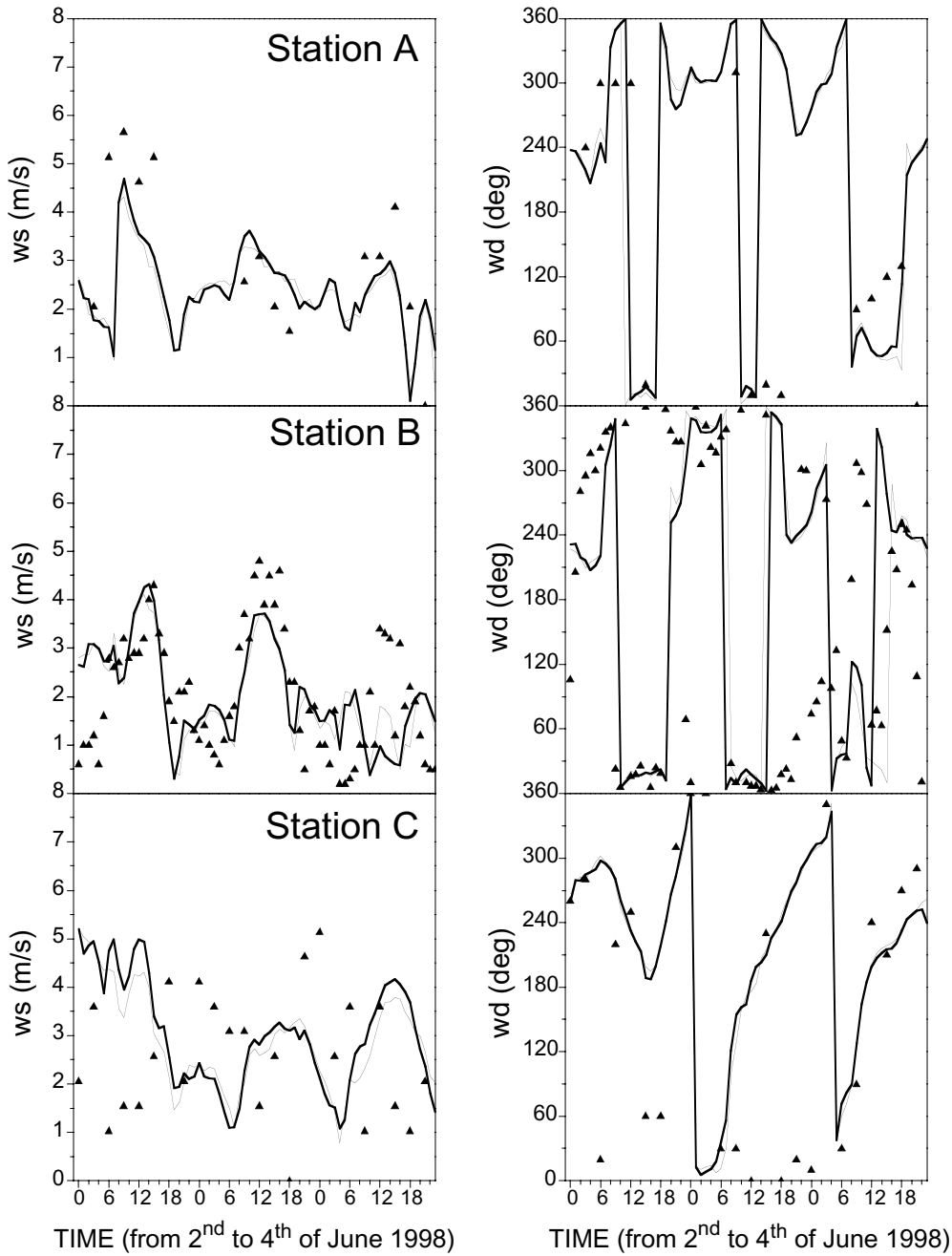


Figure 10. The evolution of modelled (lines) and observed (triangle) hourly averaged wind speed and direction at the three stations, 2–4 June 1998: thick line represents RAMS simulation with climatological SST, thin line indicates model results with SST satellite data. (Note that, in the plots of wind directions, 0° and 360° are the same.)

humidity) with the exception of wind direction, where absolute indexes are considered:

$$bias = \frac{1}{N} \sum_{i=1}^N (C_{pi} - C_{oi})$$

$$rmse = \sqrt{\frac{1}{N} \sum_{i=1}^N (C_{pi} - C_{oi})^2}$$

$$nmse \text{ (normalised mean square)} = rmse / \overline{C_p C_o}$$

$$fb \text{ (fractional bias)} = bias / (0.5(\overline{C_p} + \overline{C_o}))$$

The indexes o and p denote respectively the observed and the predicted values of meteorological fields C , and N is the number of pairs of predictions and observations made at the same time. The overbar denotes averages.

Table 3 summarises the model performance statistics for RAMS hourly averaged wind speed, wind direction, temperature and humidity simulations. The mean bias has an absolute value less than 1 m s⁻¹ for wind speed, and less than 20° for wind direction. Station B also shows the largest rmse for wind direction; this could be due to the merging of different breeze systems which

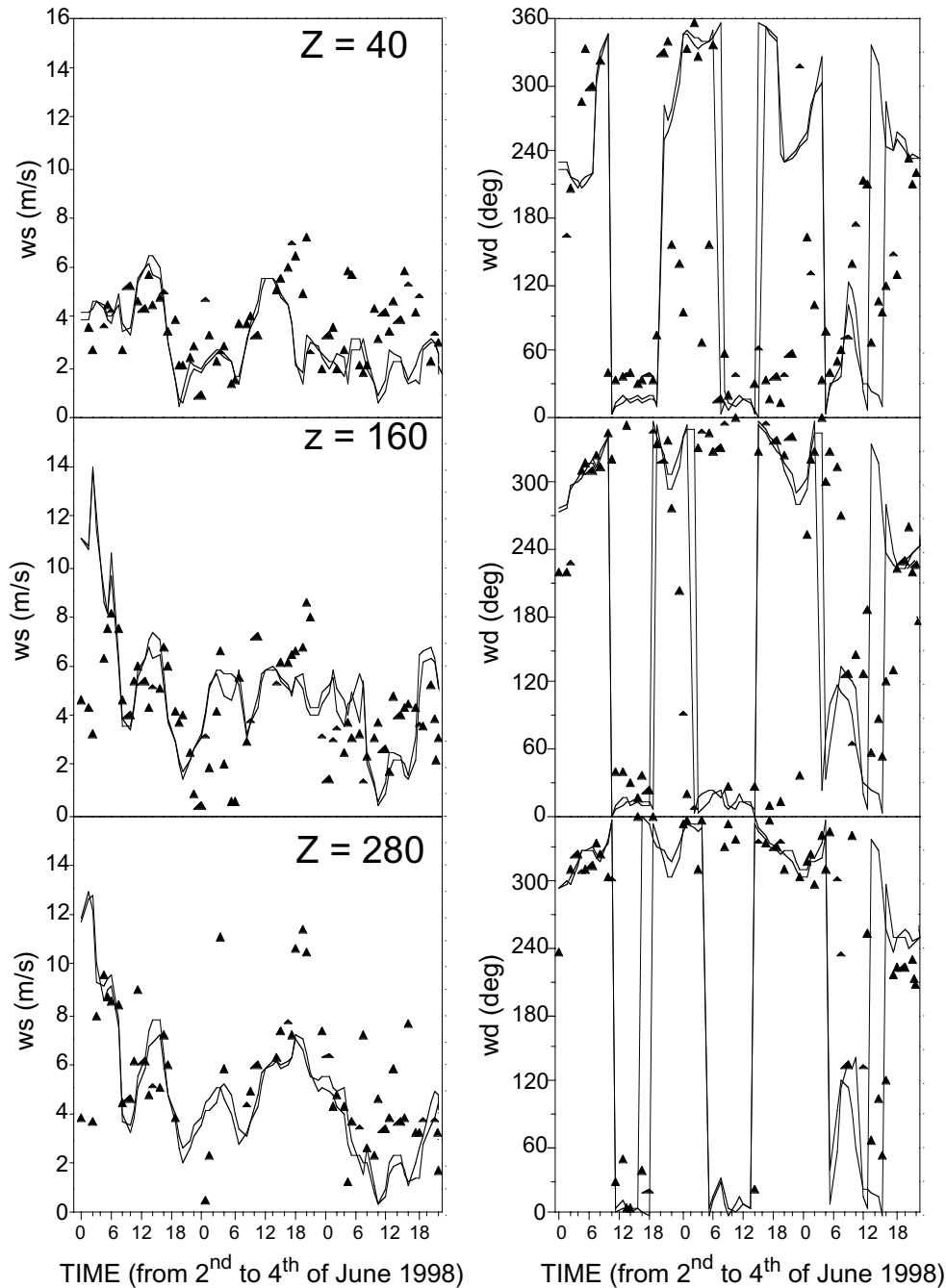


Figure 11. The evolution of modelled (lines) and sodar (triangles) hourly averaged wind speed and direction at three different measurement heights. (Note that, in the plots of wind directions, 0° and 360° are the same.)

makes the space–time matching between the model and the observations quite critical. The scatter in the sodar wind direction appears to be less than that in the corresponding surface Station B: the bias varies from -14° at $Z=50$ m to -1° at $Z=280$ m and rmse varies from 76 near the ground to 52 at $Z=280$ m. This could be due to the fact that sodar data are more representative of the model grid mesh and less sensitive to local surface effects.

Station C presents the worst statistical indexes concerning the temperature: the mean bias is -1.9°C while it is less than 1°C for the other two stations.

This may be connected to the local topographic inhomogeneities and to the poor resolution of topography.

4.2.2. Spatial statistics

In order to evaluate how the simulation performance evolves in time, spatial statistics were computed, averaging the parameters of interest over all the measurement sites. Owing to the small number of available stations, a partial (6 hour) time averaging was retained in the statistics in order to obtain the temporal

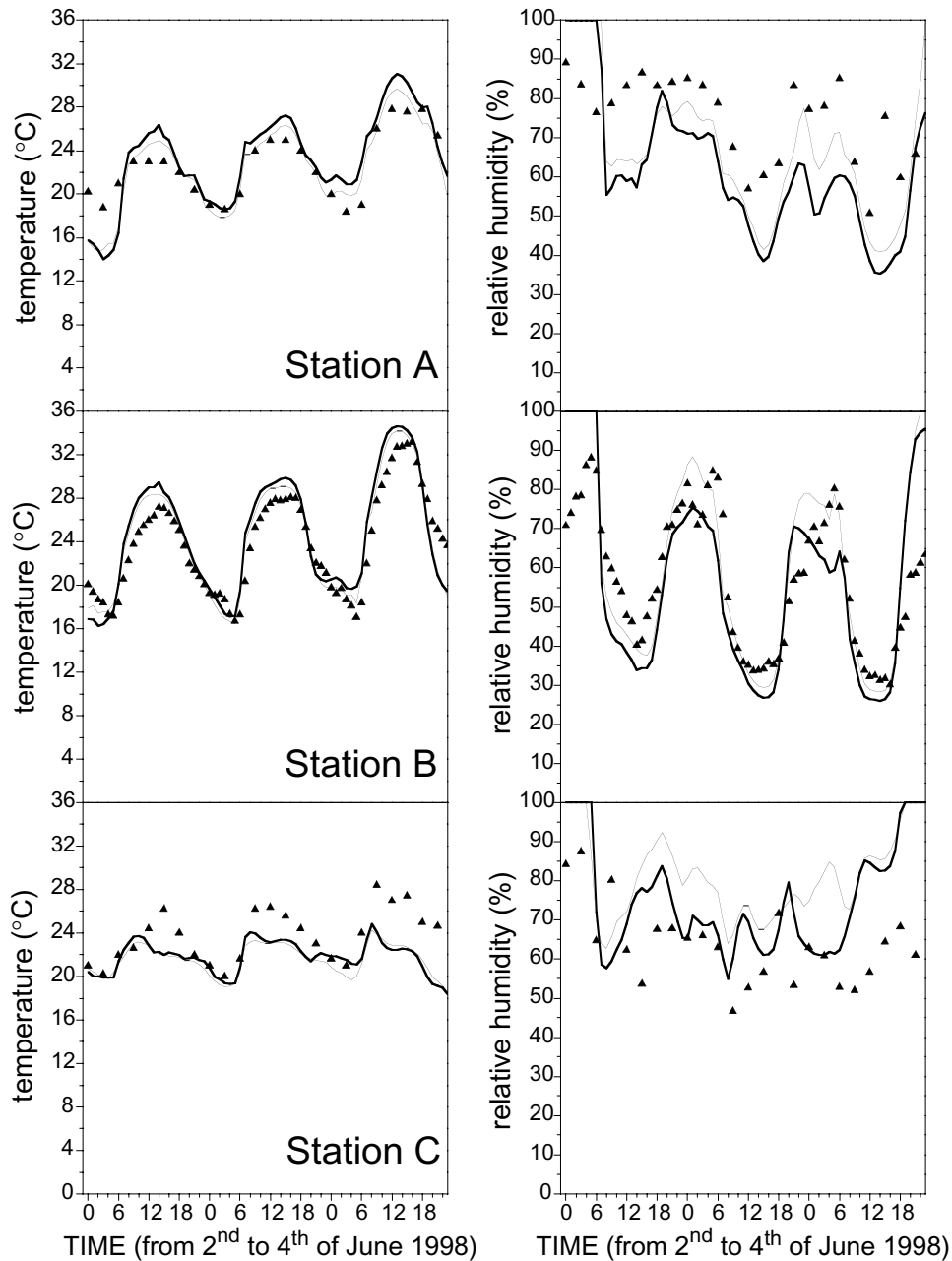


Figure 12. The evolution of modelled (lines) and observed (triangles) hourly averaged temperature and relative humidity at the three stations, 2–4 June 1998.

evolution of the significant statistical parameters with a 6-hour time step.

Figures 13 and 14 show the results of the statistical analysis for wind speed and wind direction, respectively. It can be seen that, almost every day, the wind direction bias is reduced during daytime, i.e. when wind speed is relatively high. Figures 15 and 16 illustrate the evolution of statistical indexes relating to temperature and relative humidity, respectively. A tendency to underestimate humidity is evident for most of the time.

The performance of the simulation tends to be quite good and relatively constant in time for every day except the last, when it worsens. This may be due to an

inexact timing between the actual change in the synoptic conditions that takes place on this day and the model response.

5. Conclusions

The meteorological model RAMS has been used to simulate the flow dynamics over the narrow Salento peninsula during summer conditions characterised by weak synoptic forcing. These atmospheric conditions favour the development of complex sea-breeze systems along the two coastlines, with a convergence area in the middle of the region. The selected period, 2–4 June 1998, highlights a diurnal and spatial oscillation. During

Table 3. Model performance measures for hourly averaged wind speed and direction, temperature and relative humidity, both for surface and sodar data. $bias = \frac{1}{N} \sum_{i=1}^N (C_{pi} - C_{oi})$, $rmse = \sqrt{\frac{1}{N} \sum_{i=1}^N (C_{pi} - C_{oi})^2}$, $nmse = rmse / \sqrt{C_p C_o}$, $fb = bias / (0.5(\overline{C_p} + \overline{C_o}))$. The averaging time is 1 hour.

	Station A	Station B Ground	Station B Sodar Z = 40 m	Station B Sodar Z = 160 m	Station B Sodar Z = 280 m	Station C
Wind speed mean observed (m/s)	3.4	2.1	3.93	4.58	5.90	2.7
Wind speed mean bias	-0.7	0.01	-0.8	0.5	-0.7	0.4
Wind speed rmse	1.46	1.15	1.85	2.70	2.98	2
Wind speed fractional bias	-0.16	0.00	-0.23	0.11	-0.13	0.09
Wind speed nmse	0.16	0.27	0.14	0.11	0.09	0.24
Wind direction mean bias (deg)	11	17	-14	-1	-1	5
Wind direction rmse	43	76	69	56	52	65
Temperature mean observed (°C)	22.5	23.8				23.7
Temperature mean bias	0.6	0.9				-1.9
Temperature rmse	2.3	2.2				2.7
Temperature fractional bias	0.03	0.04				-0.08
Temperature nmse	0.01	0.005				0.01
Relative humidity mean observed (%)	75	57				63
Relative humidity mean bias	-13	-1				11
Relative humidity rmse	19	14				17
Relative humidity fractional bias	-0.19	-0.02				0.16
Relative humidity nmse	0.01	0.04				0.01

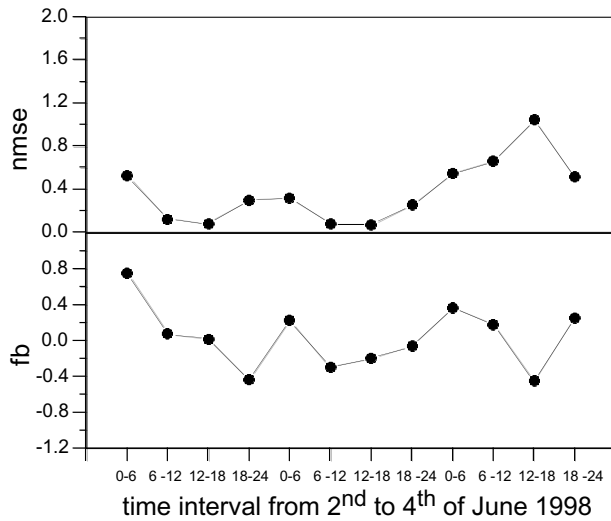


Figure 13. Wind speed: evolution of the spatial nmse (a), and fb (b), 2-4 June 1998. $nmse = \sqrt{\frac{1}{N} \sum_{i=1}^N (C_{pi} - C_{oi})^2 / \overline{C_p} \overline{C_o}}$, $fb = \frac{1}{N} \sum_{i=1}^N (C_{pi} - C_{oi}) / (0.5(\overline{C_p} + \overline{C_o}))$. The averaging times are 6 hours.

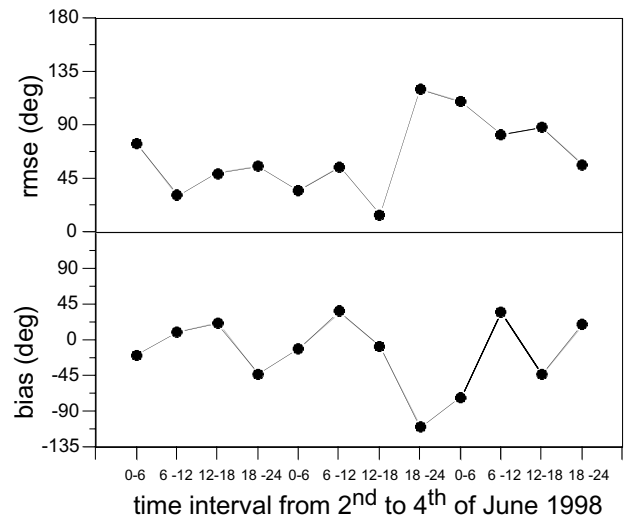


Figure 14. Wind direction: evolution of the spatial rmse (a), and bias (b), 2-4 June 1998. $rmse = \sqrt{\frac{1}{N} \sum_{i=1}^N (C_{pi} - C_{oi})^2}$, $bias = \frac{1}{N} \sum_{i=1}^N (C_{pi} - C_{oi})$. The averaging times are 6 hours.

the daytime, the wind along the two coastlines has an onshore direction, indicating the development of two distinct convergent breezes.

The structures of the thermal mixed layer and the convergence zone appear to be in general agreement with other numerical studies and with the measured data.

A comparison between the model results and the observations indicates that the model can simulate the

general mean wind field in a realistic way: it reproduces the diurnal evolution of the wind and its rotation.

The statistical evaluation highlights a quite satisfactory performance of the model for the case considered: all the values for the numerical indexes are within ranges which are characteristic of those found for other state-of-the-art models applied to other case studies (Cox et al. 1998; Hanna & Yang 2001) In particular, the model mean biases over the measurement stations are usually less than 1 m s⁻¹ for wind speed and less than 20° for wind

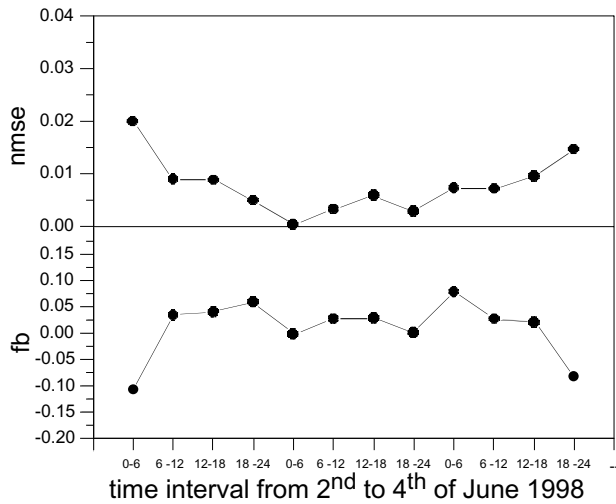


Figure 15. Temperature: evolution of the spatial $nmse$ (a), and fb (b), 2–4 June 1998. $nmse = \sqrt{\frac{1}{N} \sum_{i=1}^N (C_{pi} - C_{oi})^2 / \overline{C_p} \overline{C_o}}$, $fb = \frac{1}{N} \sum_{i=1}^N (C_{pi} - C_{oi}) / (0.5(\overline{C_p} + \overline{C_o}))$. The averaging times are 6 hours.

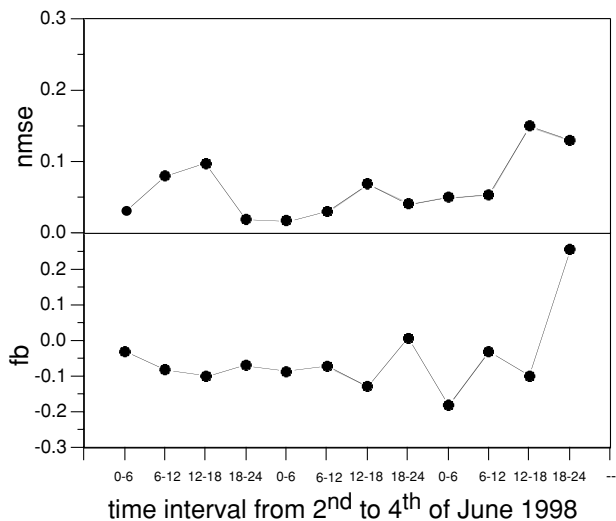


Figure 16. Relative humidity: evolution of the spatial $nmse$ (a), and fb (b), 2–4 June 1998. $nmse = \sqrt{\frac{1}{N} \sum_{i=1}^N (C_{pi} - C_{oi})^2 / \overline{C_p} \overline{C_o}}$, $fb = \frac{1}{N} \sum_{i=1}^N (C_{pi} - C_{oi}) / (0.5(\overline{C_p} + \overline{C_o}))$. The averaging times are 6 hours.

direction. The $rmse$ varies from 1 to 3 $m s^{-1}$ for wind speed and is between 50° and 70° for wind direction. This could be due to the complex wind field which makes the space–time matching between the model and the observations quite critical.

Despite a good overall agreement, there are some discrepancies at some stations. These may be in part related to the fact that the model output comprises volume averages on a horizontal $4 km \times 4 km$ grid, whereas the observations with which they are compared are point values that may in reality differ considerably from the averages. In part, these discrepancies may be due to the overlapping of sea-breeze systems which

develop over the area: the overlapping can cause too quick and localised variations of the local wind, through the rapid displacements of the merging zone, which are difficult for the model to resolve in time–space.

Spatial statistics provide evidence that: (1) the performance of the simulation tends to be quite good and relatively constant in time each day (fb and $rmse$ values are close to zero) except the last day, when it worsens: this may be related to an inexact timing between the actual change in the synoptic conditions and the model response; and (2) the deviations in wind speed and direction are reduced during daytime, i.e. when wind speed is relatively high, while the maximum deviations mostly occur during the night, being associated with calm conditions.

The use of daily data for the SST does not significantly improve the wind field calculations in this specific case, but seems to have some positive effects on the scalar variables.

Acknowledgements

The present work was partially supported by the CNR-Project CNRG00ED51 ‘Messa a punto di simulazioni meteorologiche in aree costiere tramite misure di superficie e telerilevamento’. SST data were obtained from the NASA Physical Oceanography Distributed Active Archive Center at the Jet Propulsion Laboratory, California Institute of Technology. The authors wish to thank Mr C. Elefante and Ing. G. P. Marra for their technical support, and Mr Gennaro Rispoli for supplying data for Station B. The wind climatological data are from the Italian Air Force Meteorological Service.

References

- Anthes, R. A. (1978) The height of the planetary boundary layer and the production of circulation in a sea breeze model. *J. Atmos. Sci.* **35**: 1231–1239.
- Bobyey, Z., Sethu Raman & Huang, C. (1991) Numerical simulation of sea breezes over Florida peninsula using a three dimensional planetary boundary layer model. *Am. Meteorol. Soc.* Preprints from 5th conference on Meteorology and Oceanography of the Coastal Zone. pp. 11–16.
- Brandt, J., Christensen, J. H., Frohn, L. M., Palmgren, F., Berkowicz, R. & Zlatev, Z. (2001) Operational air pollution forecasts from European to local scale. *Atmos. Environ.* **35**: 91–98.
- Cox, R., Bauer, B. & Smith, T. (1998) A mesoscale model intercomparison. *Bull. Am. Meteorol. Soc.* **79**: 265–283.
- Dalu, G. & Pielke, R. A. (1989) An analytical study of the sea breeze. *J. Atmos. Sci.* **46**: 1815–1825.
- Fisher, B. (2002) Meteorological factors influencing the occurrence of air pollution episodes involving chimney plumes. *Meteorol. Appl.* **9**: 199–210.
- Hanna, S. R. & Yang, R. (2001) Evaluation of mesoscale models’ simulation of near-surface winds, temperature gradients, and mixing depths. *J. Appl. Meteorol.* **40**: 1095–1104.

- Lyons, W. A., Pielke, R. A., Tremback, C. J., Walko, R. L., Moon D. A. & Keen C. S. (1995) Modeling impacts of mesoscale vertical motions upon coastal zone air pollution dispersion. *Atmos. Environ.* **29**: 283–301.
- Melas, D., Lavagnini, A. & Sempreviva, A. M. (2000) An investigation of the boundary layer dynamics of Sardinia Island under sea-breeze conditions. *J. Appl. Meteorol.* **39**: 516–524.
- Martano, P. (1996) Detection of mesoscale-driven circulations from time series of wind speed. *Il Nuovo Cimento* **19**: 579–590.
- Martano, P. (2002) An algorithm for the calculation of the time-dependent mixing height in coastal sites. *J. Appl. Meteorol.* **41**: 351–354.
- Nicholls, M. E., Pielke, R. A. & Cotton, W. R. (1991) A two-dimensional numerical investigation of the interaction between sea breezes and deep convection over the Florida Peninsula. *Mon. Wea. Rev.* **119**: 298–322.
- Pielke, R. A., Cotton, W. R., Walko, R. L., Tremback, C. J., Lyons, W. A., Grasso, L. D., Nicholls, M. E., Moran, M. D., Wesley, D. A., Lee, T. J. & Copeland, J. H. (1992) A comprehensive meteorological modeling system – RAMS. *Meteorol. Atmos. Phys.* **49**: 69–91.
- Pielke, R. A. & Uliasz, M. (1998) Use of meteorological models as input to regional and mesoscale air quality models – limitations and strengths. *Atmos. Environ.* **32**: 1455–1466.
- Rotunno, R. (1983) On the linear theory of the land and sea breeze. *J. Atmos. Sci.* **40**: 1999–2009.
- Seaman, N. L. (2000) Meteorological modeling for air-quality assessments. *Atmos. Environ.* **34**: 2231–2259.
- Sistla, G., Zhou, N., Hao, W., Ku, J. Y., Rao, S. T., Bornstein, R., Freedman, F. & Thunis, P. (1996) Effects of uncertainties in meteorological inputs on urban airshed model predictions and ozone control strategies. *Atmos. Environ.* **30**: 2011–2025.
- Steyn, D. G. (1998) Scaling the vertical structure of sea breezes. *Boundary-Layer Meteorol.* **86**: 505–524.
- Stull, R. B. (1988) *An Introduction to Boundary Layer Meteorology*. Kluwer Academic Publishers. 666pp.
- Walko, R. L., Tremback, C. J. & Hertenstein, R. F. A. (1995) *RAMS – The Regional Atmospheric Modeling System, Version 3b, User's Guide*. Aster Division, Mission Research Corporation, Fort Collins.
- Xian, Z. & Pielke, R. A. (1991) The effects of width of landmasses on the development of the sea breeze. *J. Appl. Meteorol.* **30**: 1280–1304.